Supporting Information

High temperature (nano)thermometers based on $LiLuF_4$: Er^{3+}, Yb^{3+} nano- and microcrystals. Confounded results for core-shell nanocrystals.

Anna M. Kaczmarek, Markus Suta, Hannes Rijckaert, Thomas P. van Swieten, Isabel Van Driessche, Mariusz K. Kaczmarek, Andries Meijerink**

Prof. A. M. Kaczmarek, Dr. H. Rijckaert, Prof. I. Van Driessche
Departement of Chemistry, Ghent University, Krijgslaan 281-S3, 9000 Ghent, Belgium.

Dr. M. Suta, T. P. van Swieten, Prof. A. Meijerink
Debye Institute, Utrecht University, Princetonplein 1, 3584 CC Utrecht, The Netherlands

Prof. M. K. Kaczmarek
Department of Mechatronics, Kazimierz Wielki University in Bydgoszcz
Kopernika 1, 85-074 Bydgoszcz, Poland

E-mail: anna.kaczmarek@ugent.be, a.meijerink@uu.nl

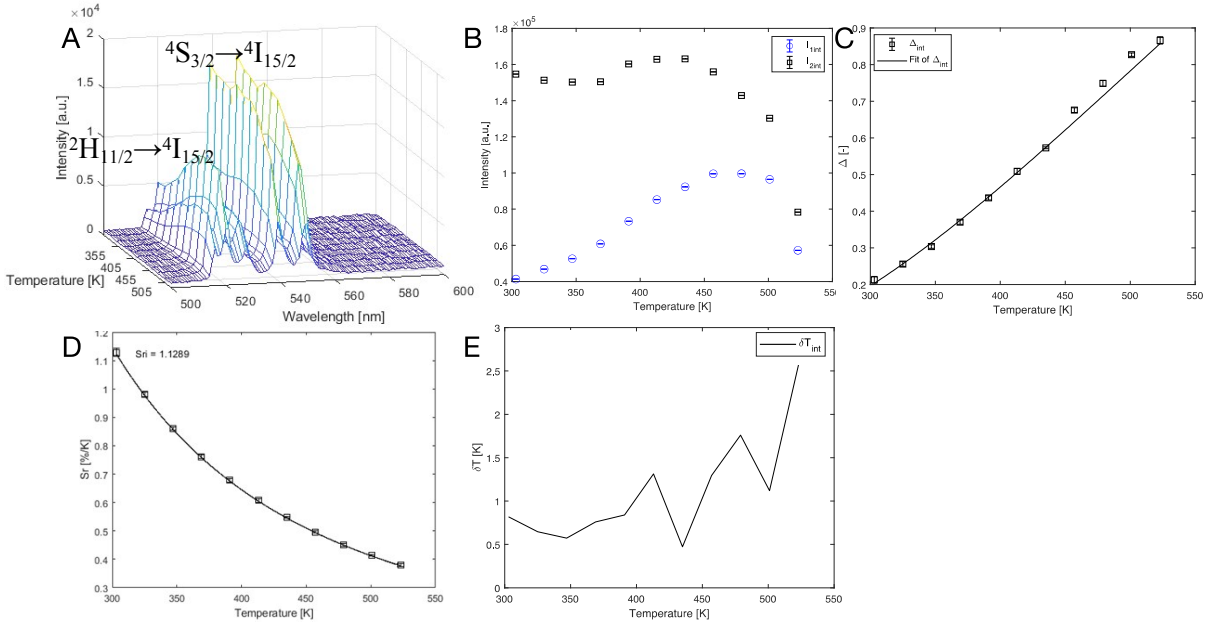

Figure S1. A) Emission map and B) values of the integrated intensities as a function of temperature (blue circles are peaks at 525 nm and black squares are the peaks at 550 nm) for $LiLuF_4$: 2% Er^{3+}, 18% Yb^{3+} core-only spherical nanocrystals. C) Plot depicting the calibration curves for the nanocrystals obtained upon usage of eqn 1. The points show the experimental Δ parameters (see eqn 1) and the solid line shows the least-squares fit of the experimental data points to the Boltzmann model (Equation 1) (ΔE = (720 ± 38) cm^{-1}, R^2 = 0.992). D) Plot of the relative sensitivity S_r at varying temperatures (303 – 523 K), the solid line is a guide for the eye. E) Graph depicting the temperature uncertainty over the regarded temperature range.

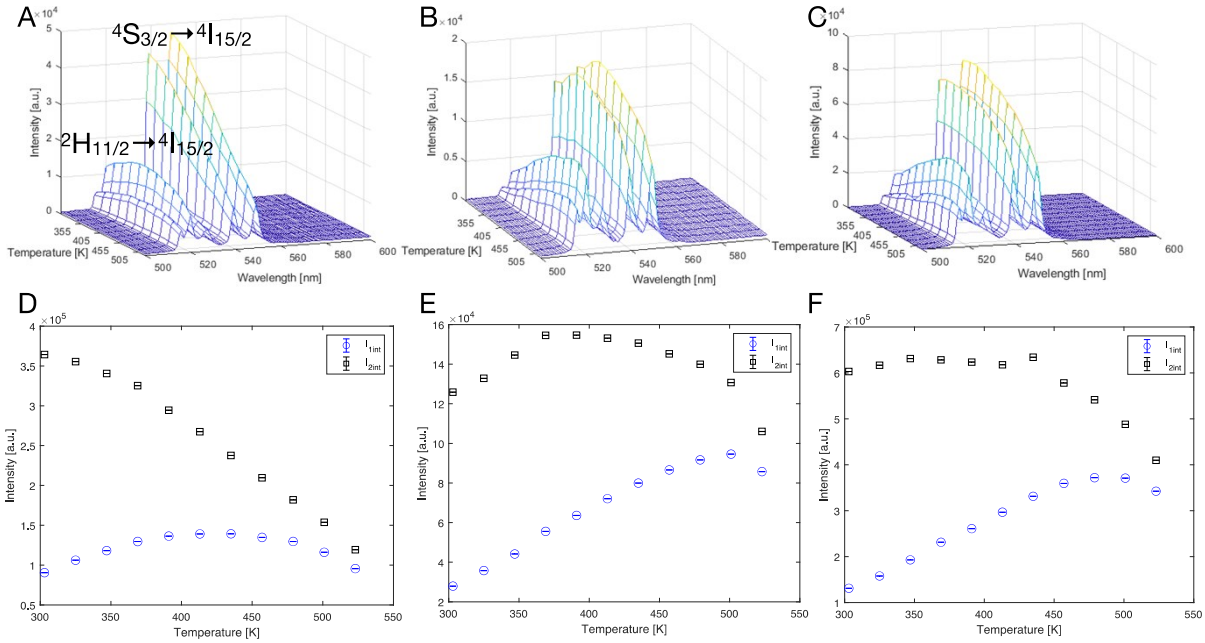

Figure S2. Emission maps and values of the integrated intensities as a function of temperature (blue circles are the peaks at 525 nm and black squares are the peaks at 550 nm) for: A) and D) $LiLuF_4$: 2% Er^{3+}, 18% Yb^{3+} core-only diamond-shaped nanocrystals, B) and E) $LiLuF_4$: 2% Er^{3+}, 18% Yb^{3+}@$LiLuF_4$ core-shell diamond-shaped nanocrystals (three shells), and C) and F) $LiLuF_4$: 2% Er^{3+}, 18% Yb^{3+}@$LiLuF_4$ core-shell diamond-shaped nanocrystals (six shells).

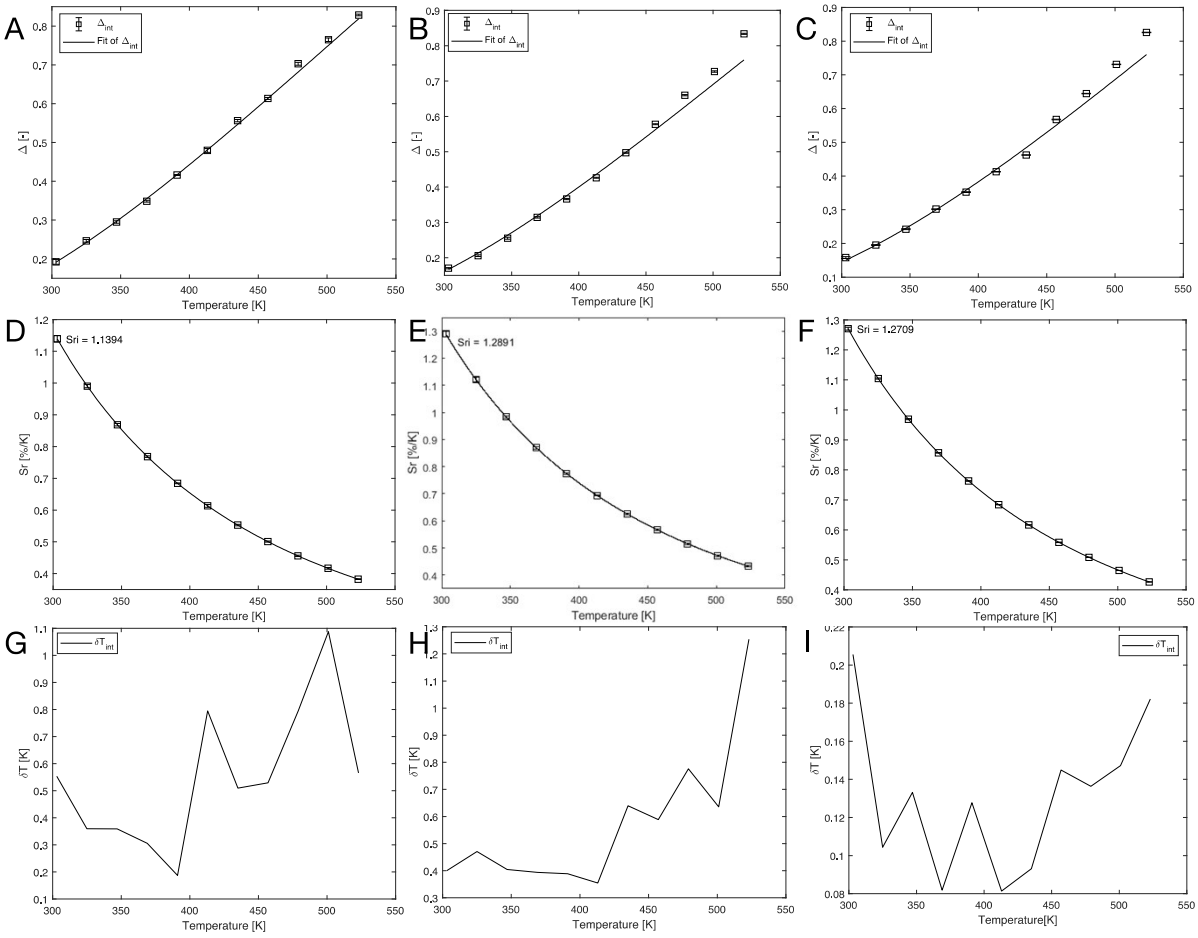

Figure S3 A), D) and G) $LiLuF_4$: 2% Er^{3+}, 18% Yb^{3+} core-only diamond-shaped nanocrystals, B), E) and H) $LiLuF_4$: 2% Er^{3+}, 18% Yb^{3+}@$LiLuF_4$ core-shell diamond-shaped nanocrystals (three shells), C), F), I) $LiLuF_4$: 2% Er^{3+}, 18% Yb^{3+}@$LiLuF_4$ core-shell diamond-shaped nanocrystals (six shells). Top: plots depicting the calibration curves for the core-only and core-shell $LiLuF_4$: 2% Er^{3+}, 18% Yb^{3+} diamond-shaped nanocrystals obtained upon usage of eqn 1. The points show the experimental Δ parameters (see eqn 1) and the solid line shows the least-squares fit to the experimental points. Middle: plots of the relative sensitivity S_r with varying temperatures (303 – 523 K), the solid lines are a guide for the eyes. Bottom: graphs depicting the temperature uncertainty over the regarded temperature range. The thermometric parameters for the compounds are compiled in Table S1.

Table S1. Overview of the thermometric parameters for the $LiLuF_4$: Er^{3+}, Yb^{3+} diamond-shaped nanocrystals.

Compound	Diamond-shaped $LiLuF_4$:Er,Yb	Diamond-shaped $LiLuF_4$:Er,Yb@$LiLuF_4$ (three shells)	Diamond-shaped $LiLuF_4$:Er,Yb@$LiLuF_4$ (six shells)
ΔE	(727 ± 19) cm^{-1}	(822 ± 63) cm^{-1}	(810 ± 64) cm^{-1}
R^2	0.998	0.987	0.985
S_r	1.1394 $\%K^{-1}$ (303 K)	1.2891 $\%K^{-1}$ (303 K)	1.2709 $\%K^{-1}$ (303 K)
δT	< 1.1 K	< 1.3 K	< 0.21 K

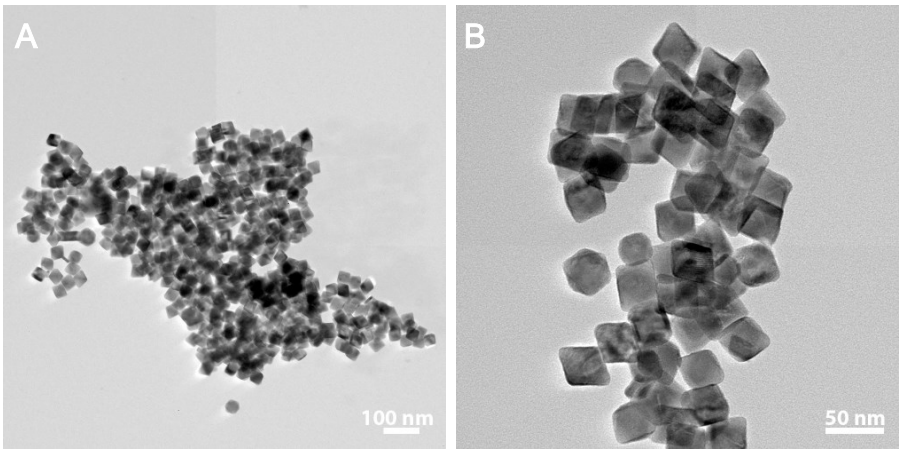

Figure S4. TEM images of $LiLuF_4$: 2% Er^{3+}, 18% Yb^{3+} core-only diamond-shaped nanocrystals after heating in the Linkam stage above 523 K.

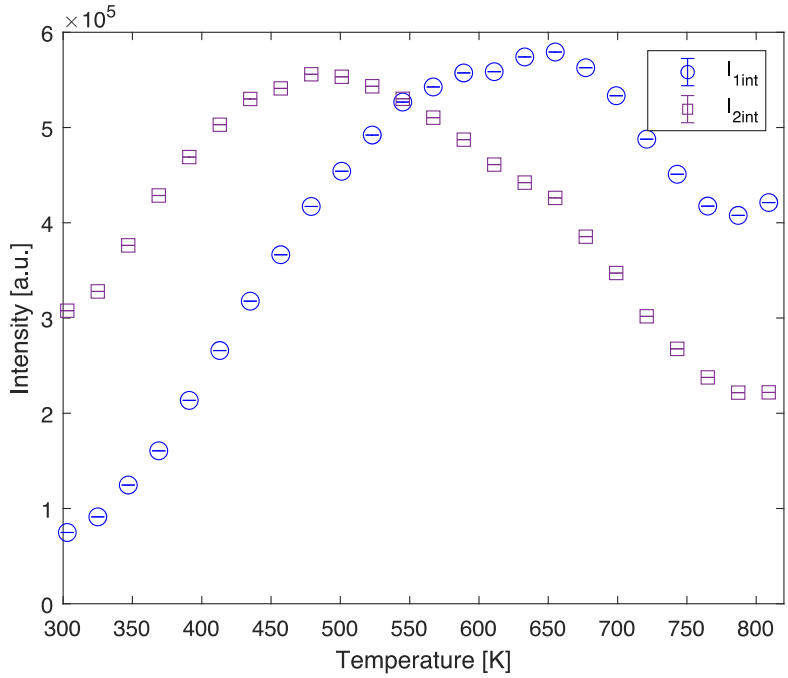

Figure S5. Values of the integrated intensities as a function of temperature (blue circles are the peaks at 525 nm and purple squares are the peaks at 550 nm) for $LiLuF_4$: 2% Er^{3+}, 18% Yb^{3+}@$LiLuF_4$@SiO_2.

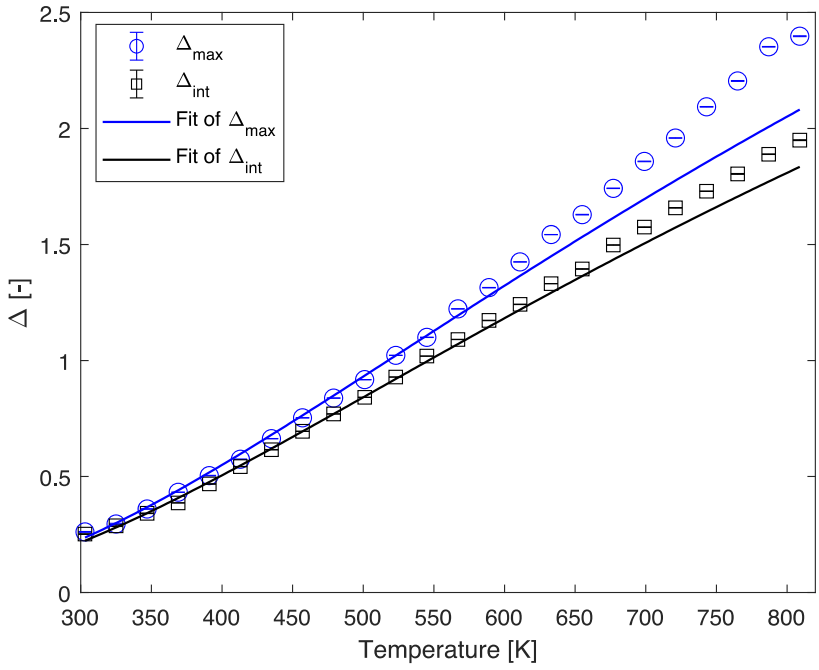

Figure S6. Plot depicting the calibration curves (blue – based on peak maxima, black – based on integrated area under the peaks) for the $LiLuF_4$: 2% Er^{3+}, 18% Yb^{3+}@$LiLuF_4$@SiO_2 nanocrystals obtained upon usage of eqn 1. The points show the experimental Δ parameters (see eqn 1) and the solid line shows the least-squares fit of eqn 1 to the experimental points.

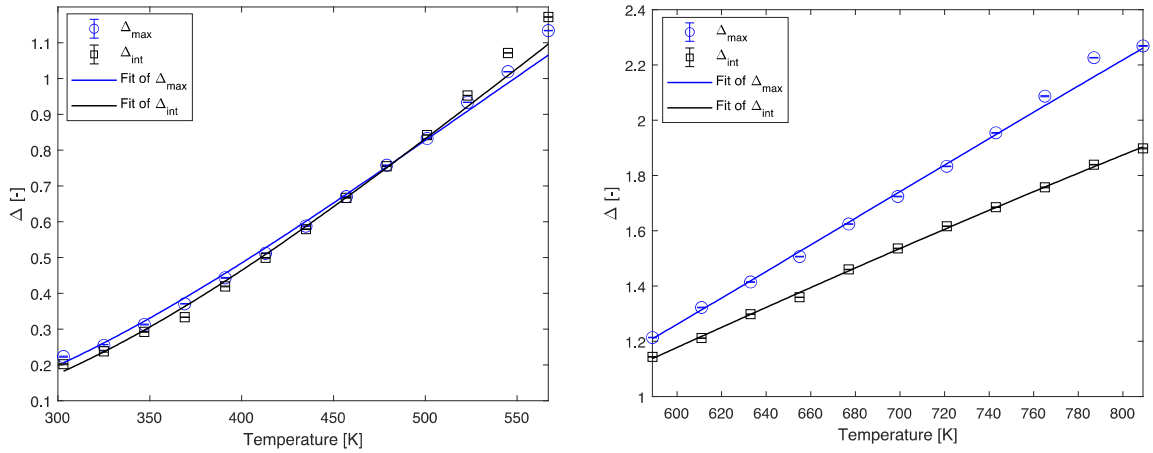

Figure S7. Plots depicting the calibration curves (blue – based on peak maxima, black – based on integrated area under the peaks) for the $LiLuF_4$: 2% Er^{3+}, 18% Yb^{3+}@$LiLuF_4$@SiO_2 nanocrystals upon usage of eqn 1 and artificial separation of the data at 567 K based on the best R^2 fits. The points show the experimental Δ parameters (see eqn 1) and the solid line shows the least-squares fit to the experimental points.

Derivation of eqn. 4 in the manuscript

Conventionally, the thermometric luminescence intensity ratio, Δ, is defined as the ratio between the intensity I or average photon count $\langle N \rangle$ measures of two radiative transitions from thermally coupled excited states to a common ground state. Since lanthanide-based transitions from a common spin-orbit level cover a wider wavelength range due to the different crystal field components, the intensity or photon count measure has to be integrated to account for the overall detected photons from a given state. We denote the overall emission intensity measure for the radiative transition $|j\rangle \rightarrow |0\rangle$ as ϕ_{j0}, which we do not specify further. Thus, Δ can be formally defined as

$$\Delta = \frac{\phi_{20}}{\phi_{10}} = \frac{\int_{\lambda_{21}}^{\lambda_{22}} d\lambda \frac{d\phi}{d\lambda}}{\int_{\lambda_{11}}^{\lambda_{12}} d\lambda \frac{d\phi}{d\lambda}}$$

It is noteworthy that dependent on the light detection principle of the employed experimental device, integration of the luminescence signal has to be performed in either an energy or wavelength scale for physically meaningful values of ϕ_{j0}. For the general proof of eqn. 4, these details are not relevant, however.

Suppose that the anticipated radiative transition "$|2\rangle \rightarrow |0\rangle$" is not pure, but actually overlaps with a third radiative transition $|3\rangle \rightarrow |0\rangle$ within the integration domain [λ_{21}, λ_{22}] and that also state $|3\rangle$ thermalizes with states $|2\rangle$ and $|1\rangle$ above a certain threshold temperature T_c (see eqn. 5 in the manuscript). The thermalization between $|3\rangle$ and $|1\rangle$ can be formally separated from that between $|2\rangle$ and $|1\rangle$, since

$$\Delta = \frac{\int_{\lambda_{21}}^{\lambda_{22}} d\lambda \frac{d\phi}{d\lambda}}{\int_{\lambda_{11}}^{\lambda_{12}} d\lambda \frac{d\phi}{d\lambda}} = \frac{\int_{\lambda_{21}}^{\lambda_{32}} d\lambda \frac{d\phi}{d\lambda} + \int_{\lambda_{32}}^{\lambda_{22}} d\lambda \frac{d\phi}{d\lambda}}{\int_{\lambda_{11}}^{\lambda_{12}} d\lambda \frac{d\phi}{d\lambda}} = \frac{\int_{\lambda_{21}}^{\lambda_{32}} d\lambda \frac{d\phi}{d\lambda}}{\int_{\lambda_{11}}^{\lambda_{12}} d\lambda \frac{d\phi}{d\lambda}} + \frac{\int_{\lambda_{32}}^{\lambda_{22}} d\lambda \frac{d\phi}{d\lambda}}{\int_{\lambda_{11}}^{\lambda_{12}} d\lambda \frac{d\phi}{d\lambda}} = \Delta_{31} + \Delta_{21}$$

if λ_{32} is within the domain [λ_{21}, λ_{22}]. The first ratio then represents the thermometric measure for thermalization between states $|3\rangle$ and $|1\rangle$, while the second ratio is the pure measure for thermalization between states $|2\rangle$ and $|1\rangle$. Since thermal coupling between two states from otherwise non-interacting ions (at least on the time scale of the non-radiative transitions between the two excited states) is governed by Boltzmann's law, eqn. 4 follows immediately,

$$\Delta = \Delta_{31} + \Delta_{21} = \alpha_{31}\exp\left(-\frac{\Delta E_{31}}{k_B T}\right) + \alpha_{21}\exp\left(-\frac{\Delta E_{21}}{k_B T}\right)$$

It is important to note that the Boltzmann equilibria between $|3\rangle$ and $|1\rangle$ as well as $|2\rangle$ and $|1\rangle$, respectively, are not mutually correlated. The double Boltzmann behavior of thermometric data is solely induced by spectral overlap of the radiative transitions $|2\rangle \rightarrow |0\rangle$ and $|3\rangle \rightarrow |0\rangle$. If the two radiative transitions are spectrally sufficiently resolved, two separate ratios can be defined, which both show single Boltzmann behavior, respectively.

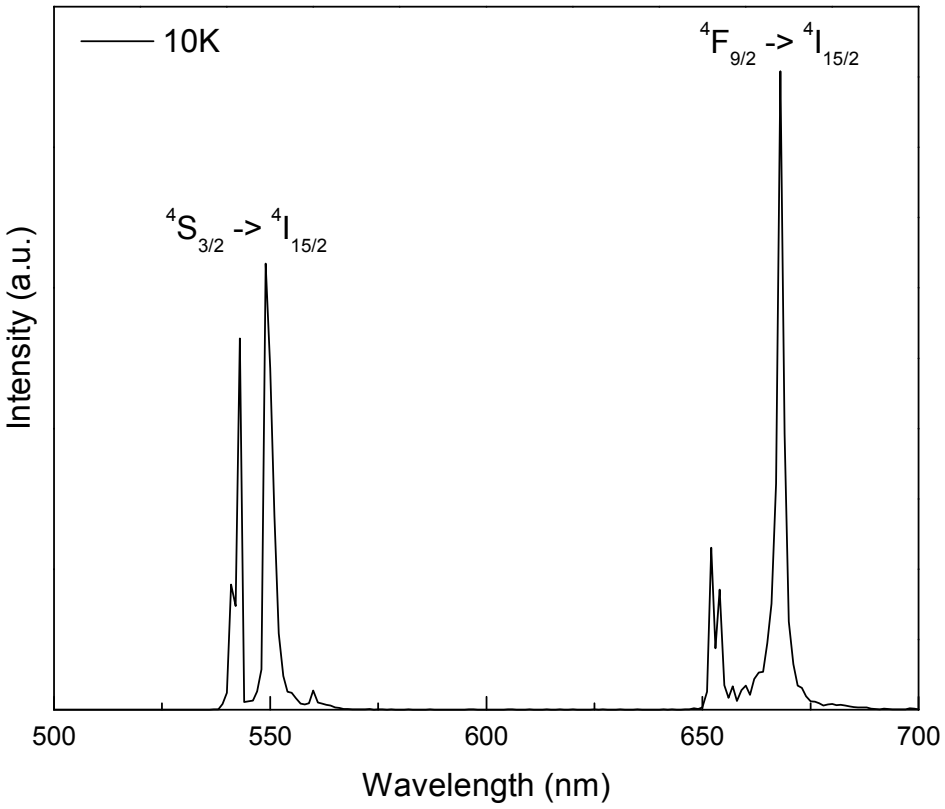

Figure S8. Emission spectrum of $LiLuF_4$: 2% Er^{3+}, 18% Yb^{3+} microcrystals recorded at 10 K.

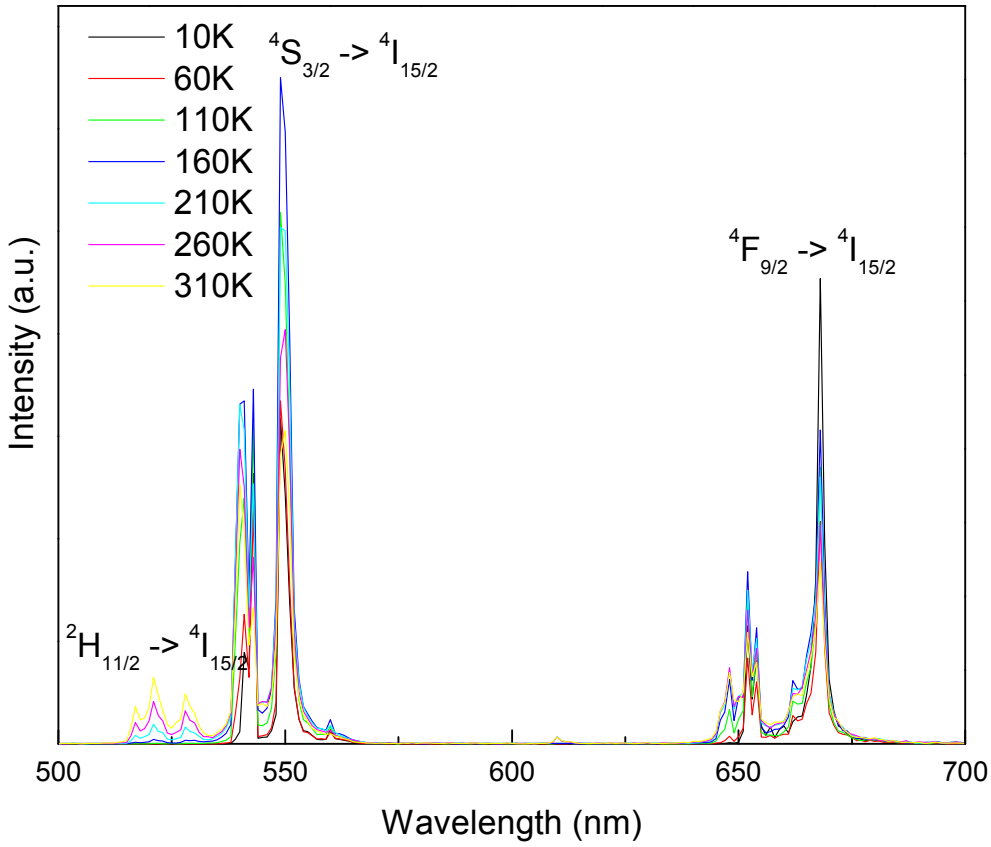

Figure S9. Emission spectra of $LiLuF_4$: 2% Er^{3+}, 18% Yb^{3+} microcrystals recorded from 10 K to 310 K.

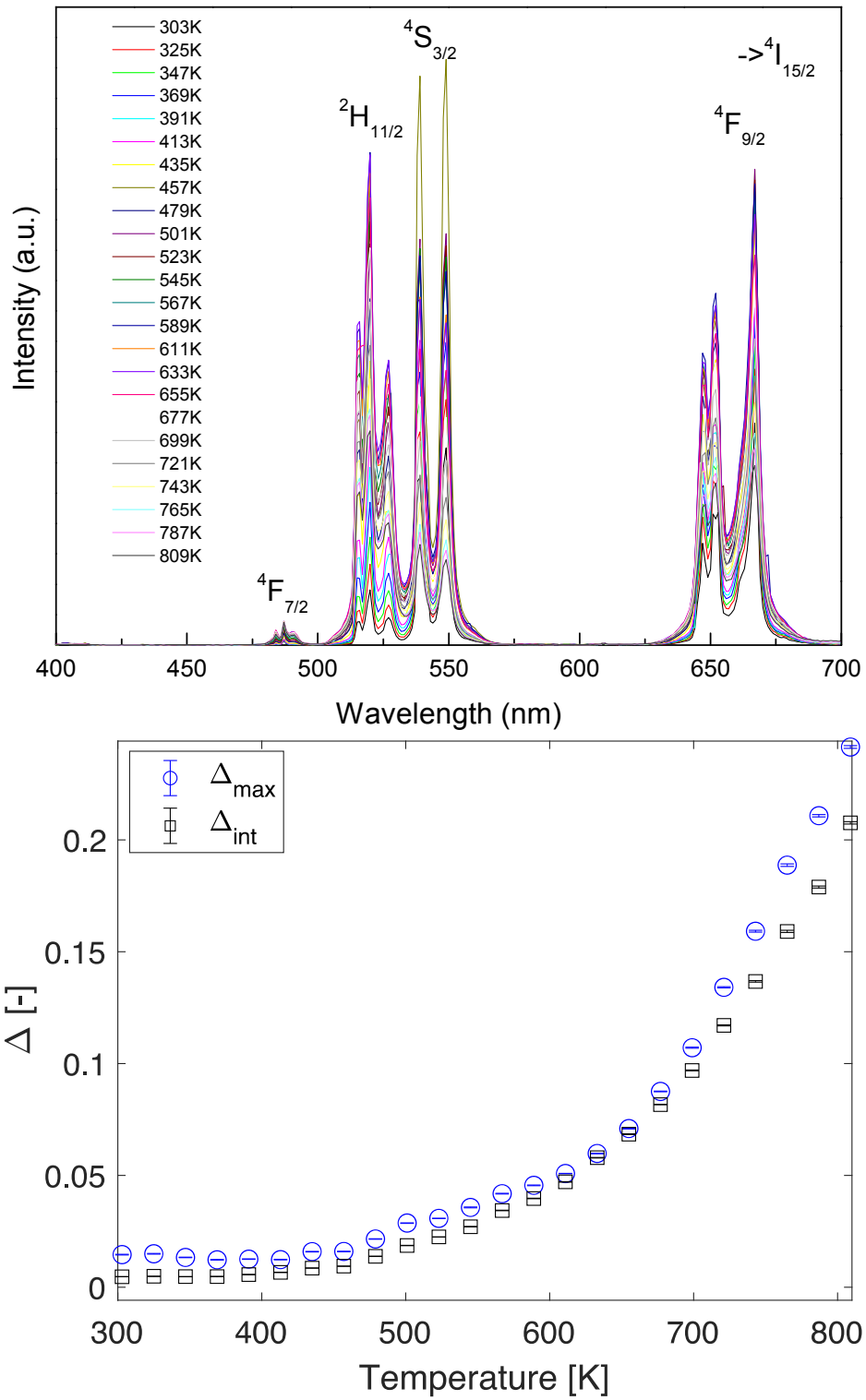

Figure S10. Top: emission spectra of $LiLuF_4$: 2% Er^{3+}, 18% Yb^{3+}@$LiLuF_4$@SiO_2 nanocrystals recorded from 400 nm to show the presence of the $^4F_{7/2} \rightarrow {}^4I_{15/2}$ transition at elevated temperatures. Bottom: curve of the Δ parameter of the $^4F_{7/2}$ and $^4S_{3/2}$ energy levels

with increasing temperature. The thermal coupling phenomenon can be observed above 500 K.

Table S2. Table compiling the α values obtained from different fitting approaches to the thermometric data of $LiLuF_4$: 2% Er^{3+}, 18% Yb^{3+}@$LiLuF_4$@SiO_2 nanocrystals and $LiLuF_4$: 2% Er^{3+}, 18% Yb^{3+} microcrystals.

Material	**Monoexponential function (eqn 1)**	**Two monoexponential functions (divided at 567 K)**	**Biexponential function (eqn 4)**
$LiLuF_4$: 2% Er^{3+}, 18% Yb^{3+}@$LiLuF_4$@SiO_2 nanocrystals	*Peak maxima:* α = 9.044	*Peak maxima:* α_1 = 8.0443 α_2 = 12.608	*Peak maxima:* α_1 = 14.436 α_2 = 3.283
	Area under peaks: α = 7.964	*Area under peaks:* α_1 = 7.997 α_2 = 9.412	*Area under peaks:* α_1 = 5.862 α_2 = 6.260
$LiLuF_4$: 2% Er^{3+}, 18% Yb^{3+} microcrystals	*Peak maxima:* α = 8.838	*Peak maxima:* α_1 = 7.713 α_2 = 13.053	*Peak maxima:* α_1 = 20.044 α_2 = 4.935
	Area under peaks: α = 7.367	*Area under peaks:* α_1 = 7.002 α_2 = 8.695	*Area under peaks:* α_1 = 6.758 α_2 = 5.4757

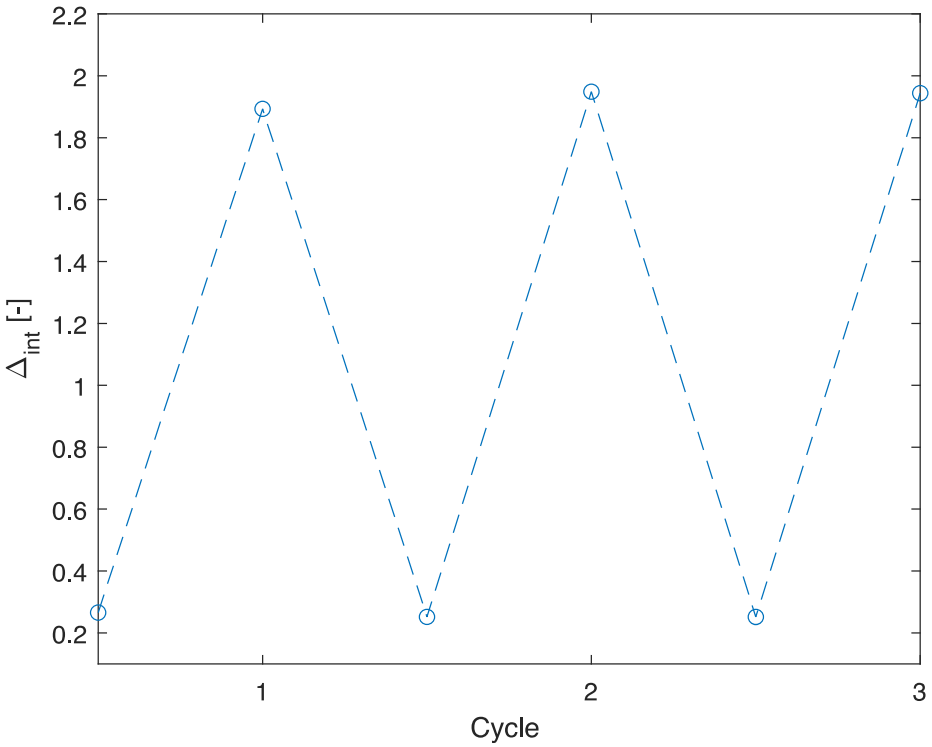

Figure S11. Cycle test for $LiLuF_4$: 2% Er^{3+}, 18% Yb^{3+}@$LiLuF_4$@SiO_2 nanocrystals. A repeatability of up to 98% was obtained. Eqn S1 was used for the calculations of the repeatability value.

$$R = 1 - \frac{max|\Delta_c - \Delta_i|}{\Delta_c} \qquad (eqn\ S1)$$

where Δ_c is the mean thermometric parameter and Δ_i is the value of each measurement of thermometric parameter.

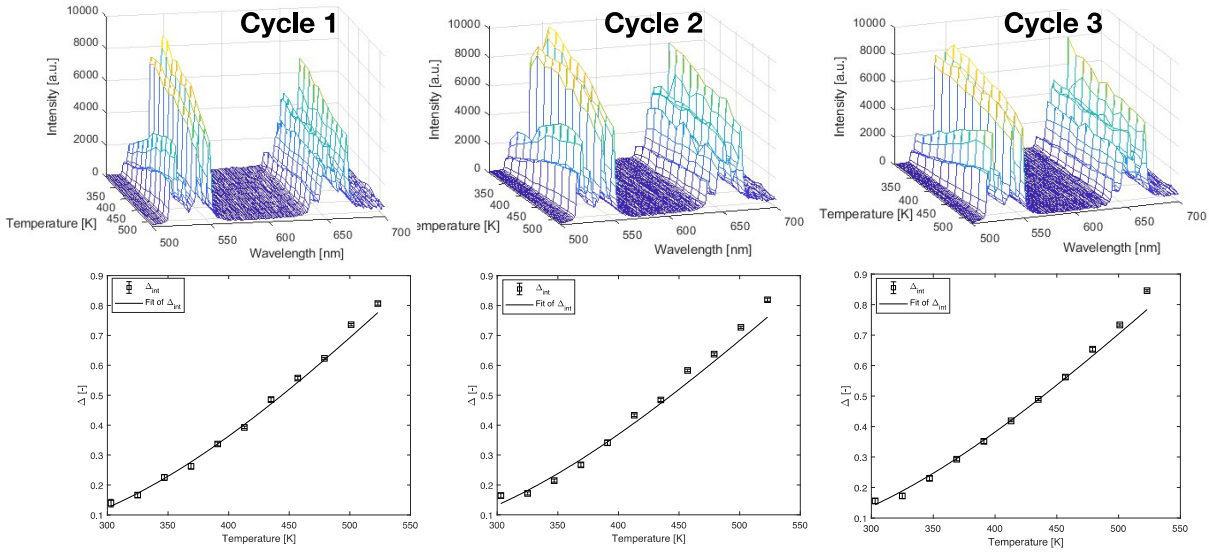

Figure S12. Cycle tests for $LiLuF_4$: 2% Er^{3+}, 18% Yb^{3+} core-only cubic nanocrystals measured in air. For each cycle, the emission map (top) and Δ plot (bottom) are depicted. The thermometric parameters for each cycle are compiled in Table S3.

Table S3. Overview of thermometric parameters for the three cycles carried out for $LiLuF_4$: 2% Er^{3+}, 18% Yb^{3+} core-only cubic nanocrystals in air.

	Cycle 1	**Cycle 2**	**Cycle 3**
Δ*E*	(896 ± 45) cm^{-1}	(855 ± 74) cm^{-1}	(849 ± 55) cm^{-1}
R^2	0.994	0.982	0.989
S_r	1.40% K^{-1} (303 K)	1.33% K^{-1} (303 K)	1.33% K^{-1} (303 K)

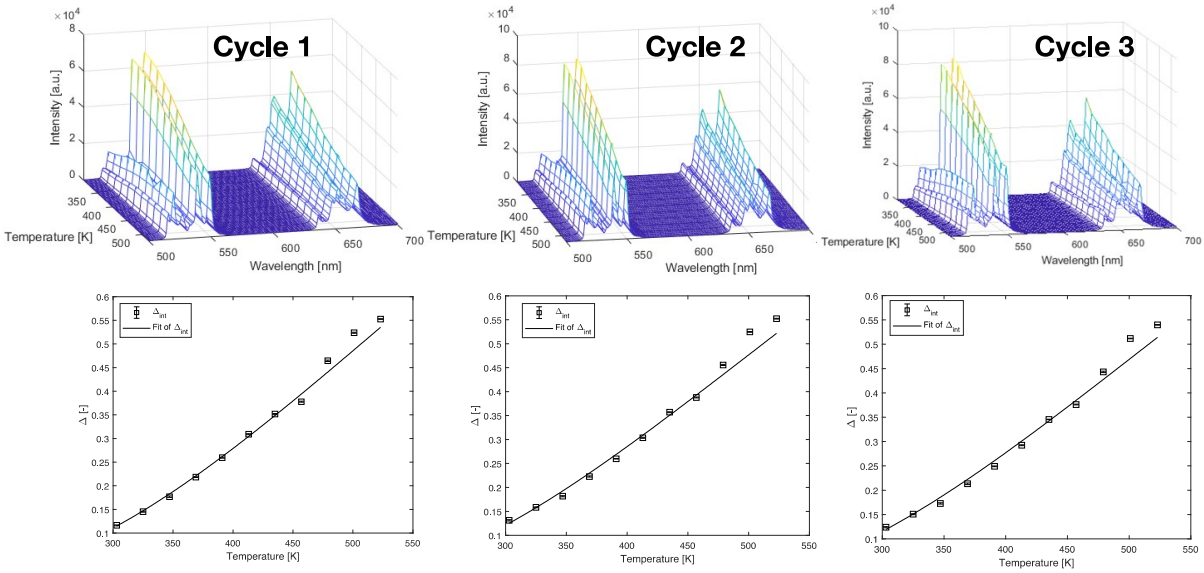

Figure S13. Cycle tests for $LiLuF_4$: 2% Er^{3+}, 18% Yb^{3+} core-only cubic nanocrystals measured in N_2. For each cycle, the emission map (top) and Δ plot (bottom) are depicted. The thermometric parameters for each cycle are been compiled in Table S4.

Table S4. Overview of thermometric parameters for the three cycles carried out for $LiLuF_4$: 2% Er^{3+}, 18% Yb^{3+} core-only cubic nanocrystals in N_2.

	Cycle 1	**Cycle 2**	**Cycle 3**
Δ*E*	(771 ± 50) cm^{-1}	(714 ± 60) cm^{-1}	(731 ± 56) cm^{-1}
R^2	0.989	0.982	0.985
S_r	1.20% K^{-1} (303 K)	1.11% K^{-1} (303 K)	1.14% K^{-1} (303 K)

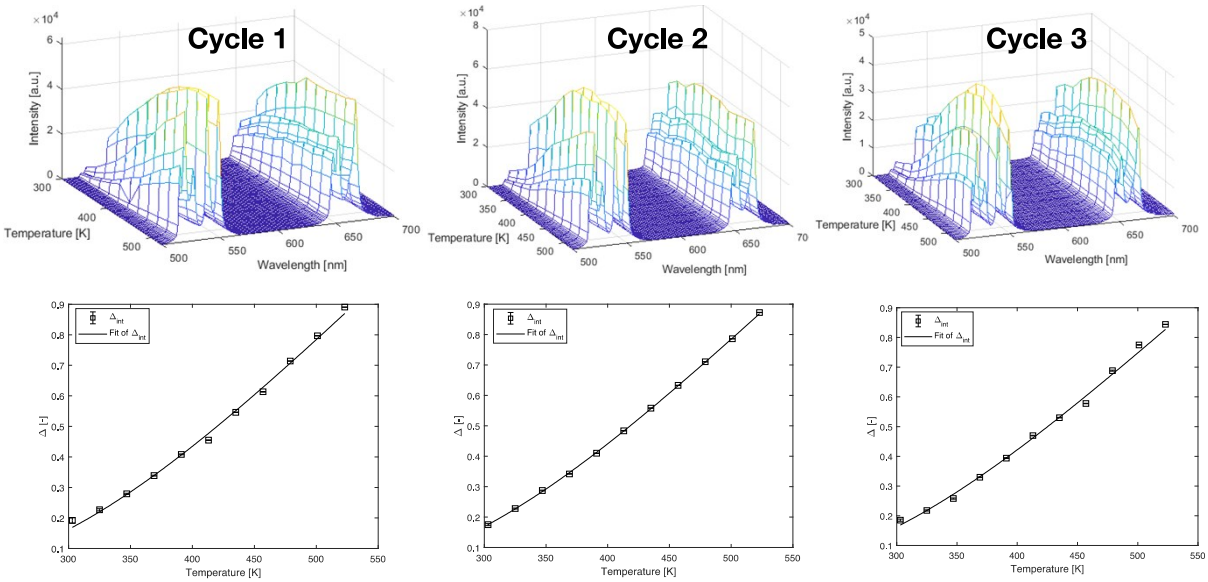

Figure S14. Cycle tests for $LiLuF_4$: 2% Er^{3+}, 18% Yb^{3+}@$LiLuF_4$ core-shell (six shells) cubic nanocrystals measured in air. For each cycle, the emission map (top) and plot (bottom) are depicted. The thermometric parameters for each cycle are compiled in Table S5.

Table S5. Overview of thermometric parameters for the three cycles carried out for $LiLuF_4$: 2% Er^{3+}, 18% Yb^{3+}@$LiLuF_4$ core-shell (six shells) cubic nanocrystals measured in air.

	Cycle 1	**Cycle 2**	**Cycle 3**
ΔE	(820 ± 28) cm^{-1}	(801 ± 5) cm^{-1}	(796 ± 31) cm^{-1}
R^2	0.997	0.999	0.996
S_r	1.28% K^{-1} (303 K)	1.25% K^{-1} (303 K)	1.24% K^{-1} (303 K)

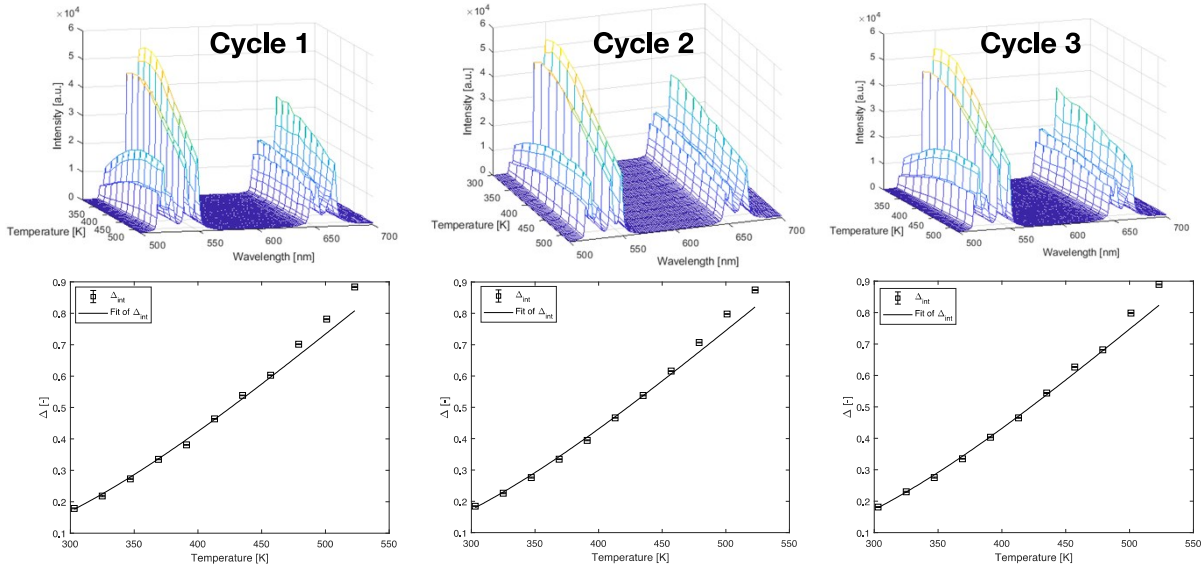

Figure S15. Cycle tests for $LiLuF_4$: 2% Er^{3+}, 18% Yb^{3+}@$LiLuF_4$ core-shell (six shells) cubic nanocrystals measured in N_2. For each cycle, the emission map (top) and Δ plot (bottom) are depicted. The thermometric parameters for each cycle are compiled in Table S6.

Table S6. Overview of thermometric parameters for the three cycles carried out for $LiLuF_4$: 2% Er^{3+}, 18% Yb^{3+}@$LiLuF_4$ core-shell (six shells) cubic nanocrystals measured in N_2.

	Cycle 1	**Cycle 2**	**Cycle 3**
ΔE	(761 ± 64) cm^{-1}	(760 ± 53) cm^{-1}	(763 ± 55) cm^{-1}
R^2	0.982	0.987	0.987
S_r	1.19% K^{-1} (303 K)	1.19% K^{-1} (303 K)	1.19% K^{-1} (303 K)

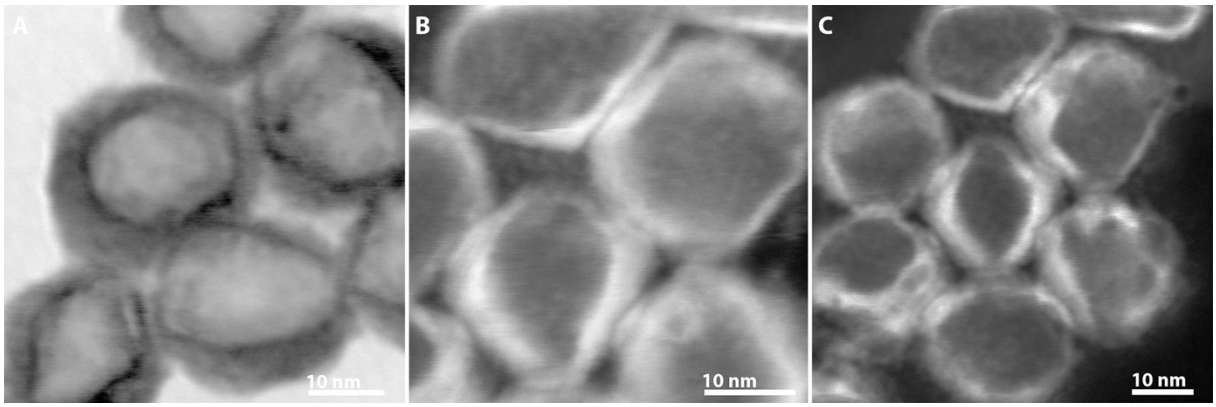

Figure S16. (S)TEM images of the $LiLuF_4$: 2% Er^{3+}, 18% Yb^{3+}@$LiLuF_4$ core-shell (six shells) cubic nanocrystals visualizing the presence of the shells.

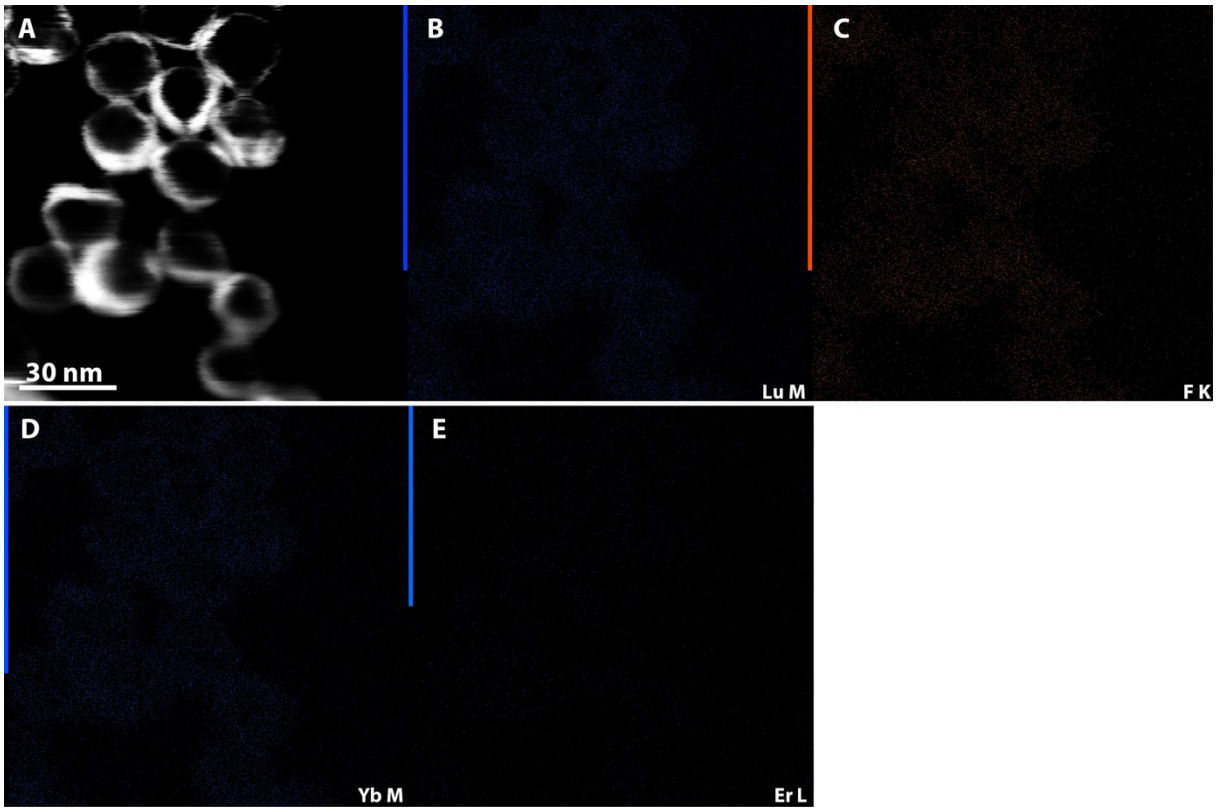

Figure S17. Additional STEM-EDX images for $LiLuF_4$: 2% Er^{3+}, 18% Yb^{3+}@$LiLuF_4$ core-shell cubic nanocrystals (six shells). The following elements were mapped: Lu (B), F (C), Yb (D) and Er (E).

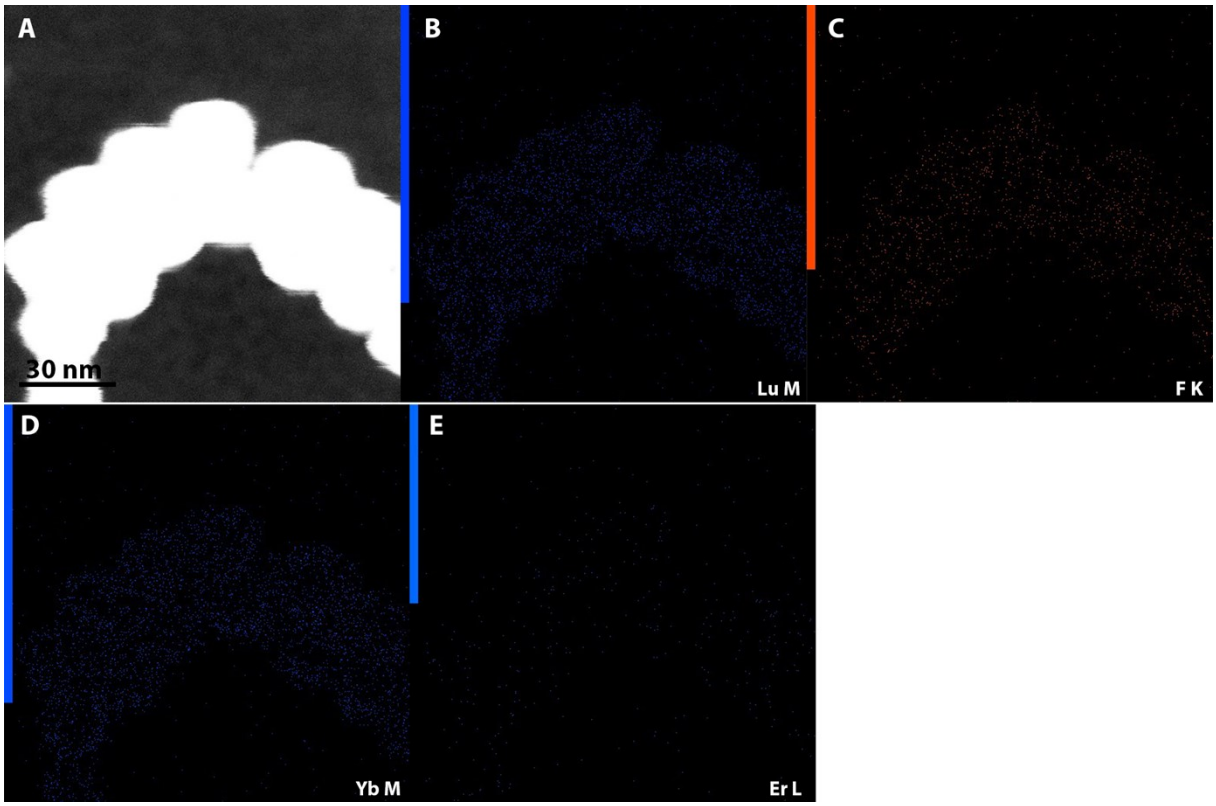

Figure S18. Additional STEM-EDX images for $LiLuF_4$: 2% Er^{3+}, 18% Yb^{3+}@$LiLuF_4$ core-shell cubic nanocrystals (six shells). The following elements were mapped: Lu (B), F (C), Yb (D) and Er (E).

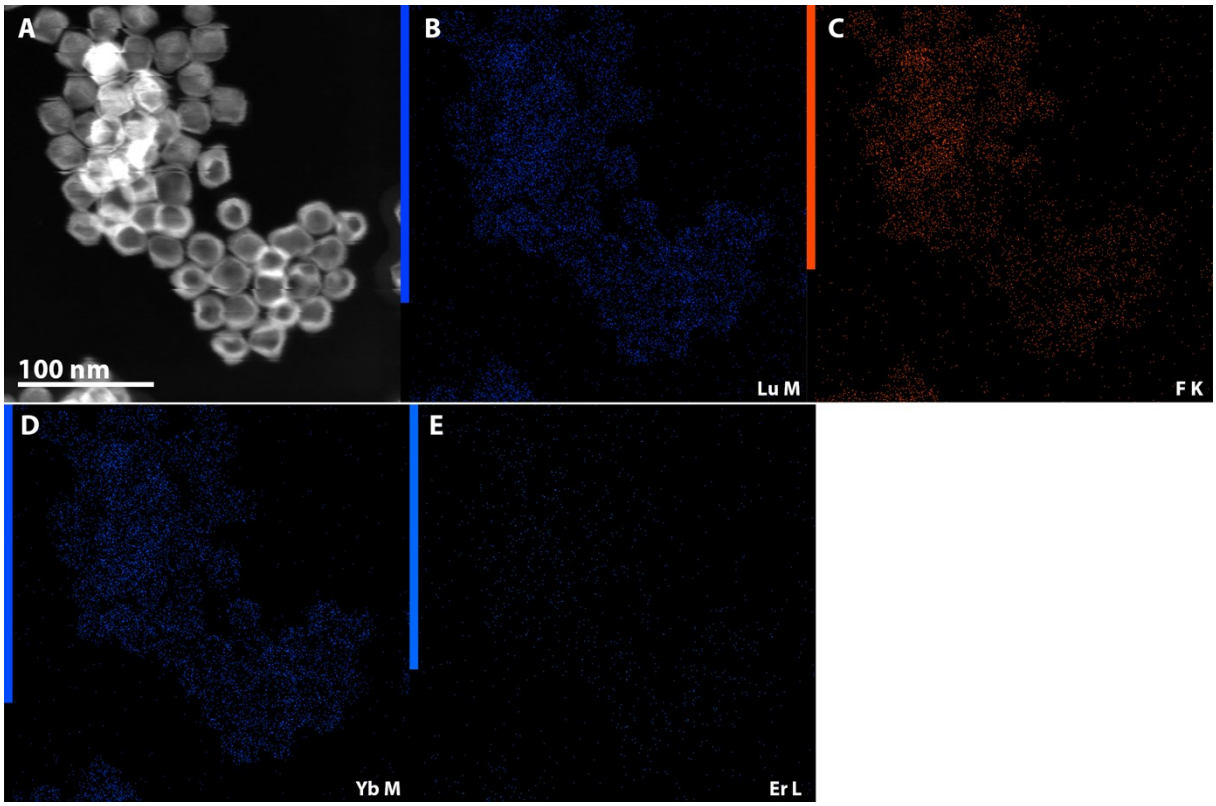

Figure S19. STEM-EDX images for $LiLuF_4$: 2% Er^{3+}, 18% Yb^{3+} core-only cubic nanocrystals synthesized in a prolong synthesis time. The following elements were mapped: Lu (B), F (C), Yb (D) and Er (E).

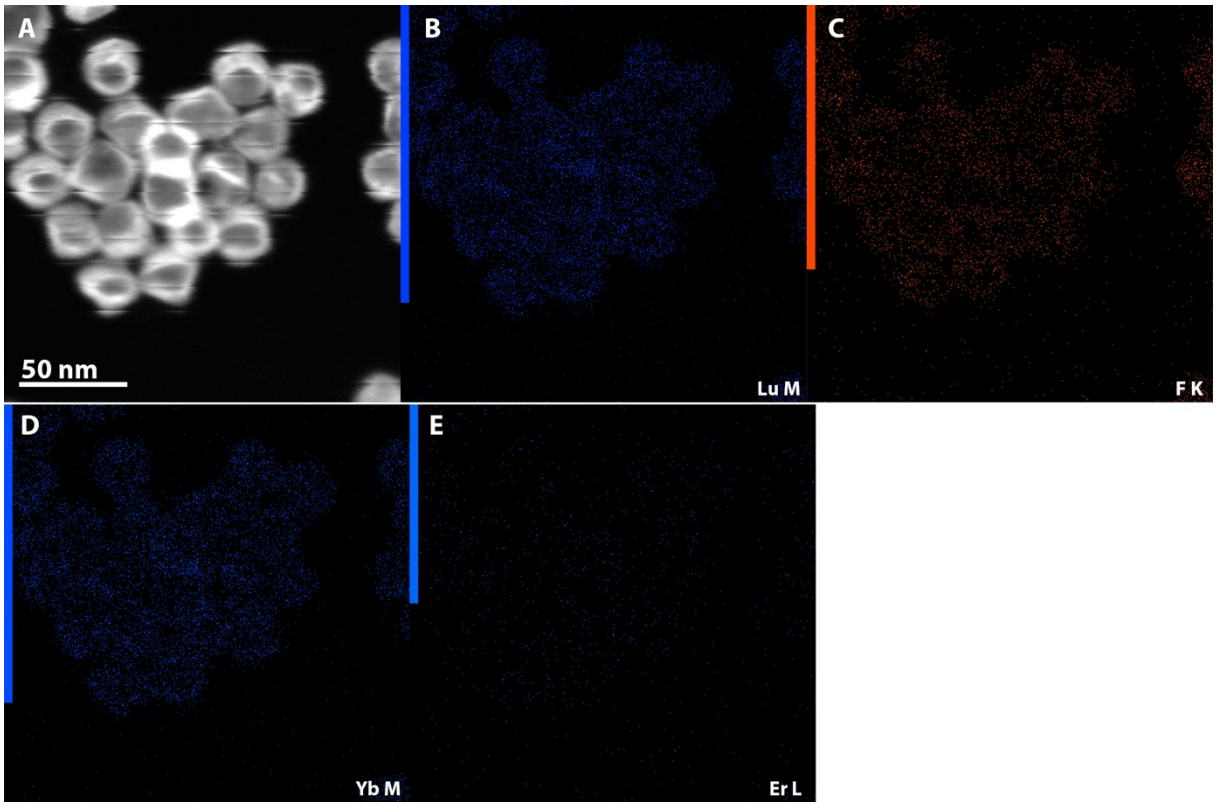

Figure S20. Additional STEM-EDX images for $LiLuF_4$: 2% Er^{3+}, 18% Yb^{3+} core-only cubic nanocrystals synthesized in a prolong synthesis time. The following elements were mapped: Lu (B), F (C), Yb (D) and Er (E).

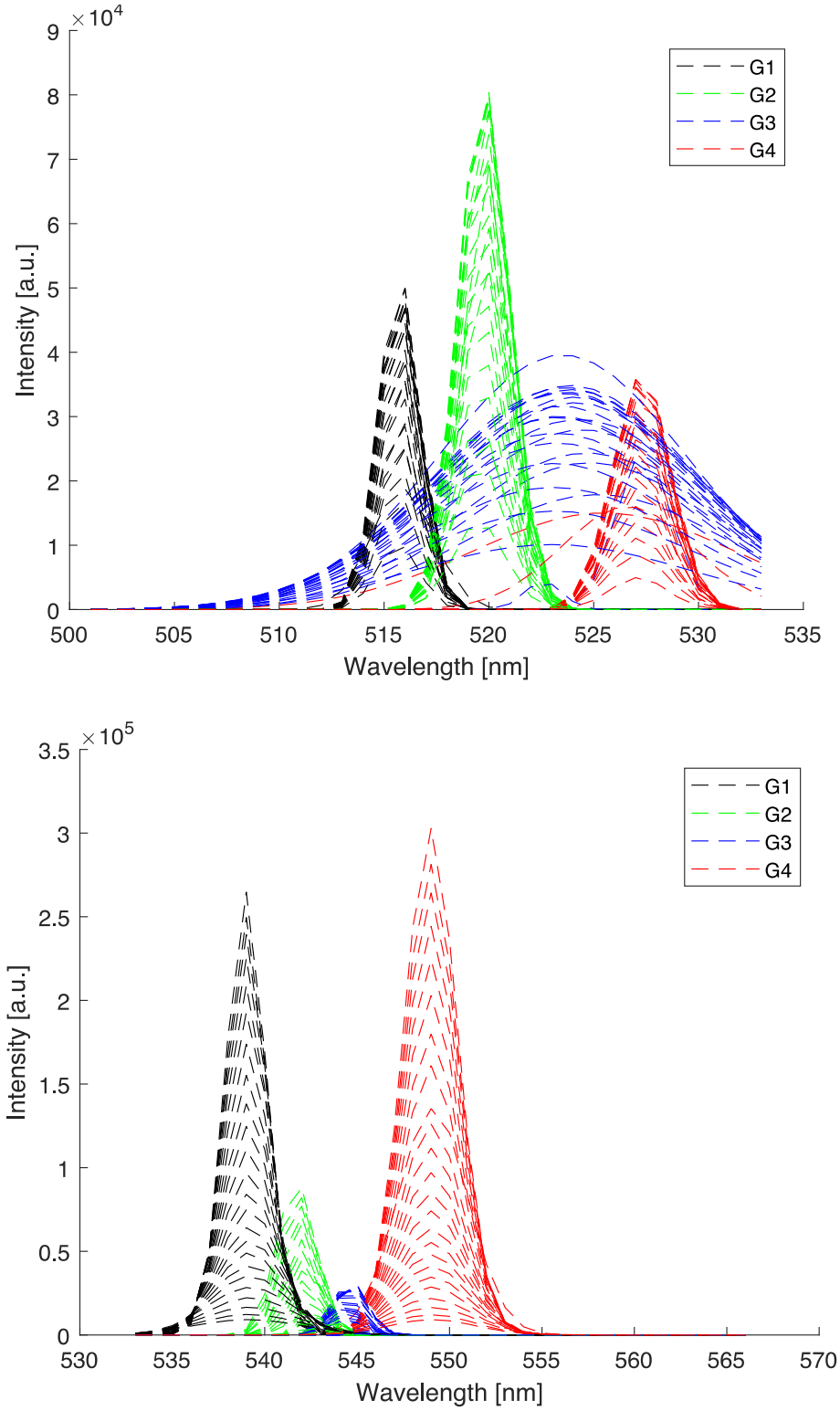

Figure S21. Example of Gaussian fits for $LiLuF_4$: 2% Er^{3+}, 18% Yb^{3+} microcrystals (for each peak 4 Gaussians were employed for the best fit, Matlab software was employed for this purpose).